Electronic Supplementary Material (ESI) for Energy & Environmental Science.

Supporting Information

Zinc/Selenium Conversion Battery: A System Highly Compatible to both Organic and Aqueous Electrolytes

Ze Chen,[1] Funian Mo,[1] Tairan Wang,[1] Qi Yang,[1] Zhaodong Huang,[1] Donghong Wang,[1] Guojing Liang,[1] Ao Chen,[1] Qing Li,[1] Ying Guo,[1] Xinliang Li,[1] Jun Fan,[1] Chunyi Zhi*[1,2]

[1]Department of Materials Science and Engineering, City University of Hong Kong, 83 Tat Chee Avenue, Kowloon, Hong Kong 999077, China.

[2]Centre for Functional Photonics, City University of Hong Kong, Kowloon, Hong Kong

E-mail: cy.zhi@cityu.edu.hk

Experimental Section

Materials: selenium powder (Se), ordered mesoporous carbon (CMK-3), zinc di[bis(trifluoromethylsulfonyl)imide] (ZnTFSI), acetonitrile (AN), ethyl methyl carbonate (EMC), dimethyl sulfoxide (DMSO), polyethylene glycol (PEG, HO(CH2CH2O)*n*H, *Mn*=600) are purchased from Aladdin. All chemicals are analytically pure and used as received without any further purification. Ultrapure water (18.2 MΩ· cm^{-1}) was used directly from Milli-Q water system.

Preparation of Se/CMK-3 cathode: A 3:7 weight ratio mixture of CMK-3 and Se bulk powder was mixed through wet ball-milling in acetone at 800 r/min for 2 h. After evaporating acetone in air at room temperature, the mixture was pressed into a pellet at 10 MPa and then calcined at 260 °C for 12 h in a sealed stainless steel autoclave filled with Ar to get the Se/CMK-3 composite.

To prepare the cathode, firstly mixing Se/CMK-3, acetylene blacks and PVDF binder (8:1:1) together in NMP to form a homogeneous slurry, which was then casted onto a piece of carbon cloth followed by drying at 65 °C. The effective mass loading of Se/CMK-3 is about 2.1 mg cm^{-2} and 10.4 mg cm^{-2}. In addition, pure Se powder was also used as the active material to prepare the bulk Se powder cathode following the same procedures (the ratio of Se : acetylene blacks : PVDF is 7:2:1), where the loading mass of Se is 8.2 mg cm^{-2}.

Characterization methods: Transmission electron microscope (TEM) and high-resolution transmission electron microscope (HRTEM) analysis was performed on a JEOL-2001F operated at 200 kV. A field-emission scanning electron microscope (SEM, FEI Quanta 450 FEG) was used to investigate the morphologies and elemental compositions of the products. Thermogravimetric analysis (TGA) of both Se/CMK-3 and CMK-3 was applied on TG/DTA 6300 to obtain the Se content in the composite. To calculate the surface area and pore volumes, the nitrogen absorption

and desorption isotherms were measured at 77.3 K on an Autosorb-1 specific surface area analyzer from Quantachrome Instruments. Phase composition transition was confirmed by X-ray diffraction equipment (XRD, Bruker D2 Phaser) with Cu Ka radiation at 30 kV, and the data were collected from 5 ° to 90 ° at a scanning speed of 5 ° min^{-1}, with a step interval of 0.02 °, respectively. X-ray photoelectron spectroscopy (XPS, ESCALAB 250) was employed to analyze the elements components of Se composites and electrode surface elements changes at different states. Raman spectra were recorded with a WITec alpha300 access with a laser of 532 nm wavelength.

Electrochemical measurements: Both coin-2032 and pouch cell were assembled for electrochemical measurements. The coin cell used a zinc foil with 0.2 mm thickness as the anode electrode, Se/CMK-3 on carbon clothes with 2.1 mg cm^{-2} loading mass as the cathode, 270 μL of 1 M ZnTFSI in different solvents (EMC, AN and DMSO) as the non-aqueous electrolytes and glass fiber membrane as the separator. In addition, an aqueous electrolyte, 2M ZnTFSI/PEG/water was prepared based on the volume of the mixture of PEG-600 and deionized water, where the weight ratio of PEG-600 and deionized water is 85:15. The aqueous coin cells use the same electrode and separators mentioned above. For pouch cells, zinc foil with 0.1mm thickness as the anode, pure Se bulk powder and Se/CMK-3 composite on the carbon clothes with 8.2 mg cm^{-2} and 10.4 mg cm^{-2} loading mass as the anode, respectively, the weight ratio of Zn anode and active materials Se was set as 1.9:1. 2M ZnTFSI/PEG/water as the electrolytes and non-woven as the separator. Four batteries are assembled in parallel. The cyclic performance, electrochemical properties of batteries were characterized by the LAND CT2001A device and electrochemical workstation CHI 760D at 25 °C.

Simulation Methods: The Zn-ion solvent free energy is calculated by the cluster-continuum

model.[1] Such model separates the solvent environment around Zn-ion into inner- and outer-shell. The inner shell wherein the explicit solvent molecules forms cluster with Zn-ion is treated quantum mechanically, while the out shell is treated as dielectric continuum model (implicit solvent molecule). The solvation free energy of Zn-ion can be calculated according to

$$\Delta G^{*}_{solv}(Zn^{2+}) = \Delta G^{*}_{solv}(Zn^{2+}(X)_n) + \Delta G^{\circ}_{gas}(Zn^{2+}(X)_n) - n\Delta G^{*}_{solv}(X) - n\Delta G^{\circ\rightarrow *}$$

where X is the specific solvent molecule, n is the number of solvent molecules which form cluster with Zn-ion, and $\Delta G^{*}_{solv}(Zn^{2+}(X)_n)$ is the solvation free energy of clustered Zn-ion. $\Delta G^{\circ}_{gas}(Zn^{2+}(X)_n)$ is the cluster formation free energy in gas phase. $G^{*}_{solv}(X)$ is the solvation free energy of solvation molecules. $\Delta G^{\circ\rightarrow *}$ is the free energy difference between standard-states and equals 1.9 Kcal mol^{-1}. The configurations of initial Zn-solvent cluster are generated by the global optimization code, ABCluster.[2] Then the computationally efficient optimization is carried out in Gaussian09 under B3LYP/6-31G* level to obtain the lowest-energy cluster from 20 candidates. The lowest-energy cluster is further optimized under B3LYP-D3BJ/6-311G** level to reach a more accurate structure. The free energy contribution is also calculated under the same level. All these optimizations and free energy calculations are performed in Polarizable Continuum Model using the integral equation formalism variant (IEFPCM). The dielectric constant is set to 35.688 for Acetonitrile, 78.355 for Water, 46.826 for DMSO and 3.500 for EMC.[3] To assess the accurate cluster formation energy in gas phase, the single point energy of fully optimized structures is calculated under B2PLYPD3/def2TZVP level. The solvation free energy of fully optimized clustered Zn-ion and solvent molecular is calculated under M052X/6-31G* level.

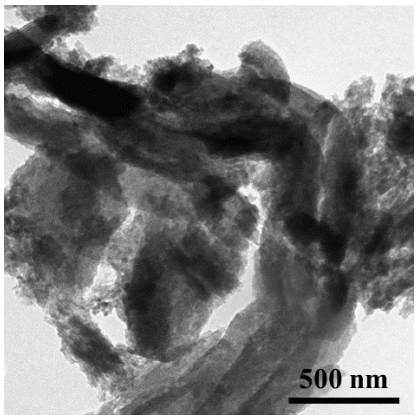

Figure S1. TEM image of Se/CMK-3 composites.

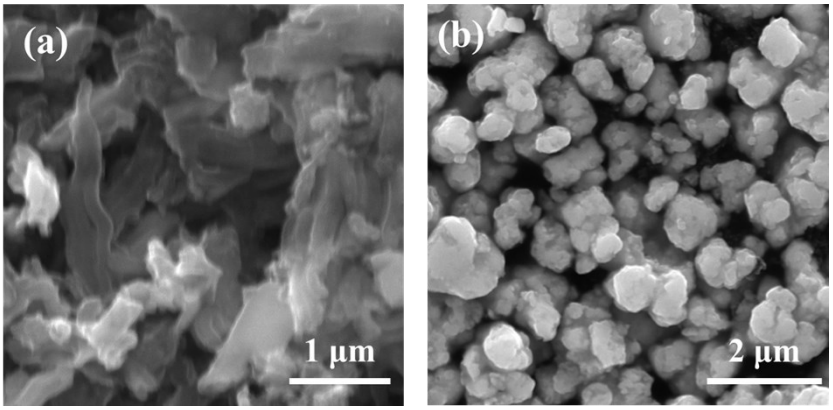

Figure S2. SEM images of a) CMK-3 and b) Se bulk powder.

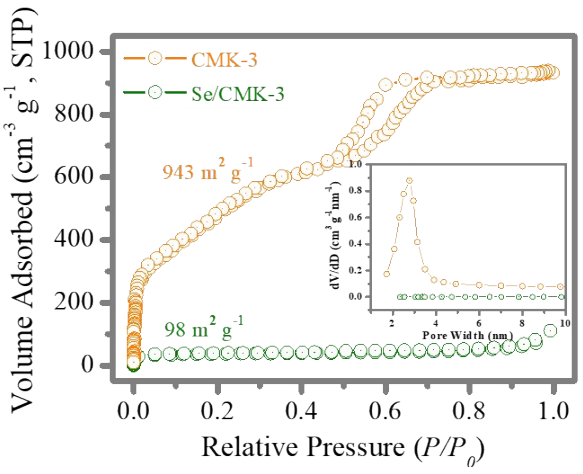

Figure S3. Nitrogen adsorption-desorption isotherms and pore size distributions of CMK-3 and the Se/CMK-3 composite.

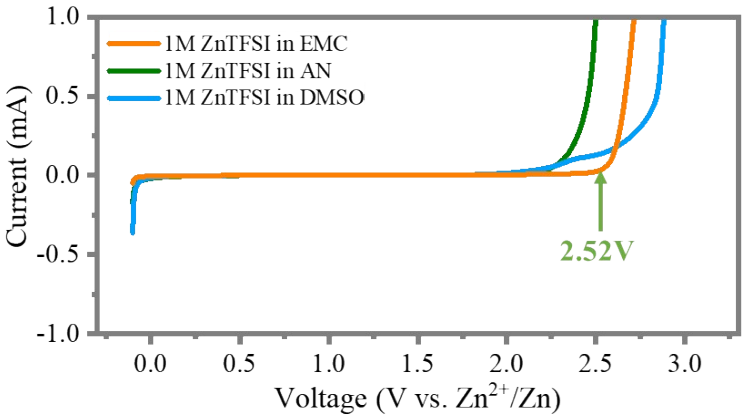

Figure S4. LSV curves of different organic electrolytes with the scan rate of 1 mV s^{-1}.

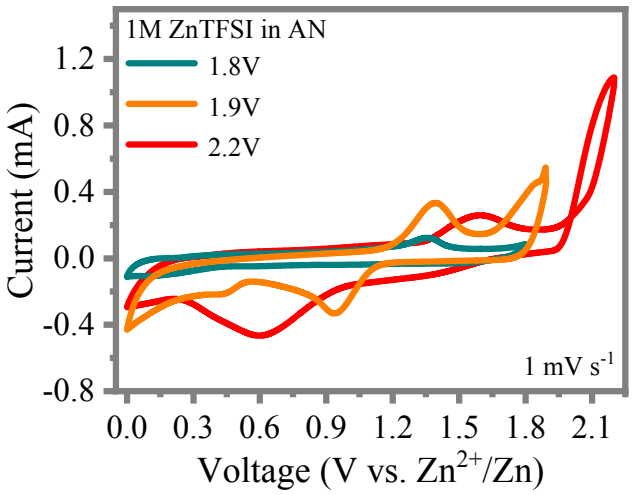

Figure S5. CV curves of Zn-Se batteries with AN based organic electrolytes within different voltage windows.

From the CV curves with different voltage windows, AN based electrolyte shows obvious decomposition behavior when being charged to 2.2V though it output larger discharge capacity. It indicates the AN based electrolyte is not appropriate for the Zn-Se batteries. The main reason for such a CV curve is the intermediate polyselenides continuously shuttle to the anode when charged to a higher voltage and react with Zn metal.

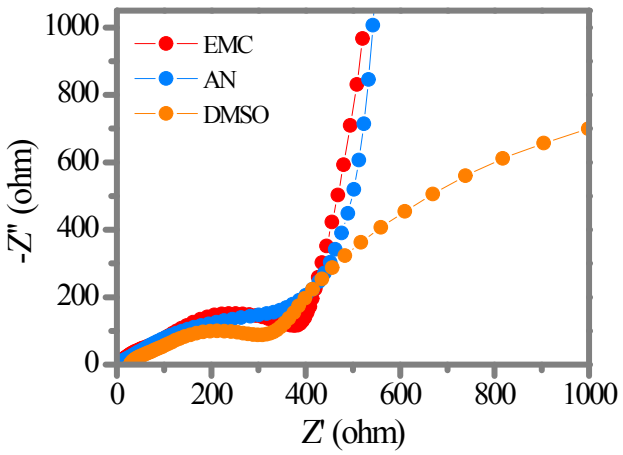

Figure S6. EIS test of Zn-Se batteries based on three different electrolytes.

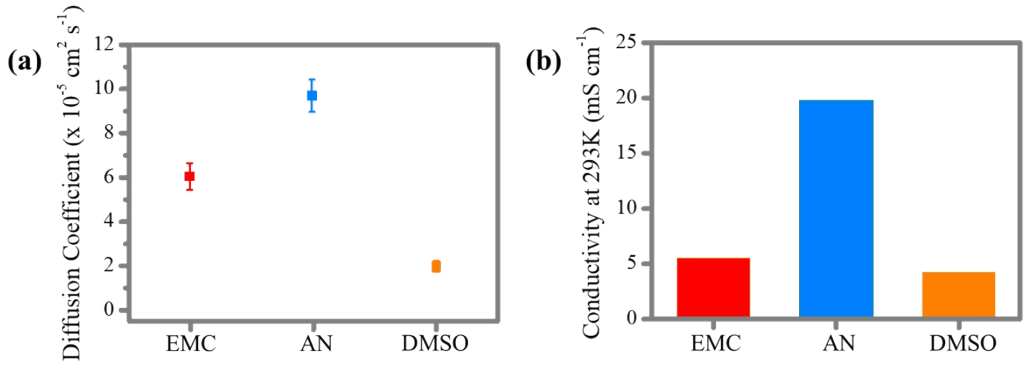

Figure S7. a) Isothermal diffusion coefficients of 1M ZnTFSI in EMC, AN and DMSO (from experimental estimation methods at 293K), respectively. b) Ion conductivity of 1M ZnTFSI in EMC, AN and DMSO.

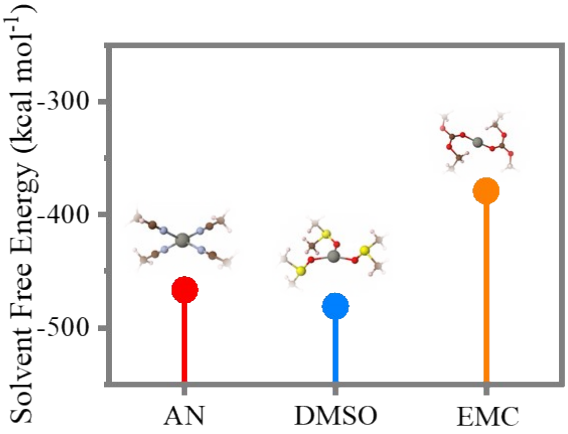

Figure S8. Calculation of Zn^{2+} solvent free energy under different solvent environment: AN, DMSO and EMC, respectively.

The Zn^{2+} solvent free energy is calculated by the cluster continuum model and the calculated energy ΔG of the three different solvent environment AN, DMSO and EMC are -466.65, -481.11 and -378.94 kcal mol^{-1}, respectively.

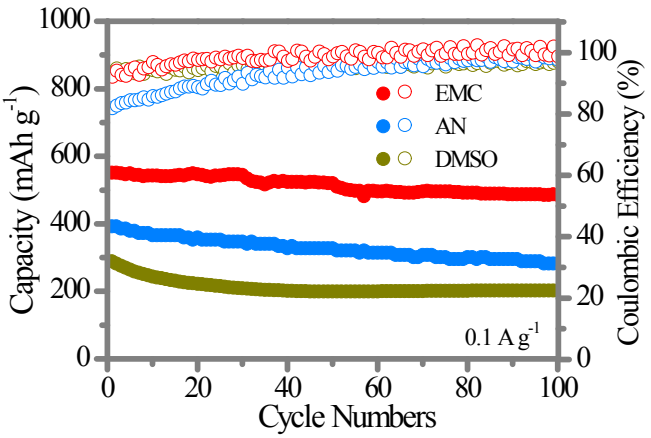

Figure S9. Preliminary cycling performance test of the Zn-Se batteries with three different electrolytes for 100 cycles at 0.1 A g^{-1}.

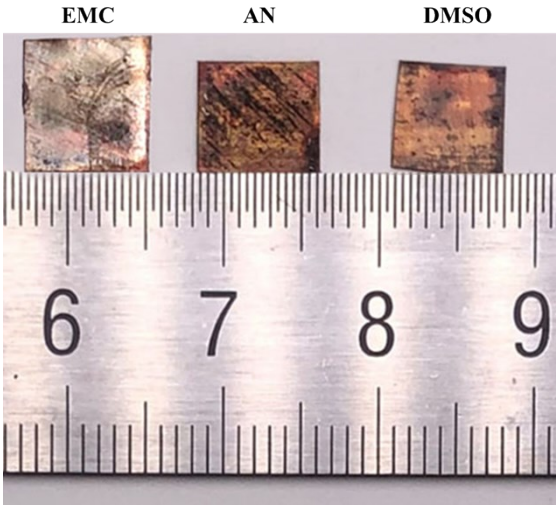

Figure S10. Pictures of Zn anode after 100 cycles under 1M ZnTFSI in EMC, AN and DMSO based electrolytes, respectively.

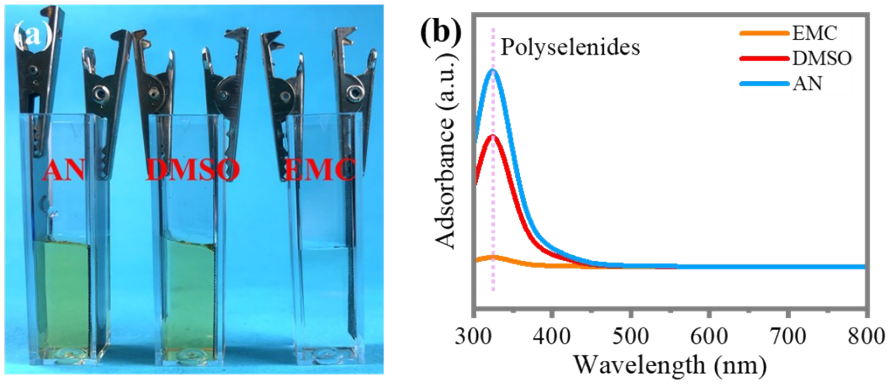

Figure S11. a) Picture of the Zn-Se batteries based on different organic electrolytes after 50 cycles; b) UV-vis tests of the organic electrolytes confirm the content of polyselenides after 50 cycles. It can be found that AN and DMSO based electrolytes exhibit severe shuttle effect, but EMC based electrolytes shows much weaker shuttle effect.

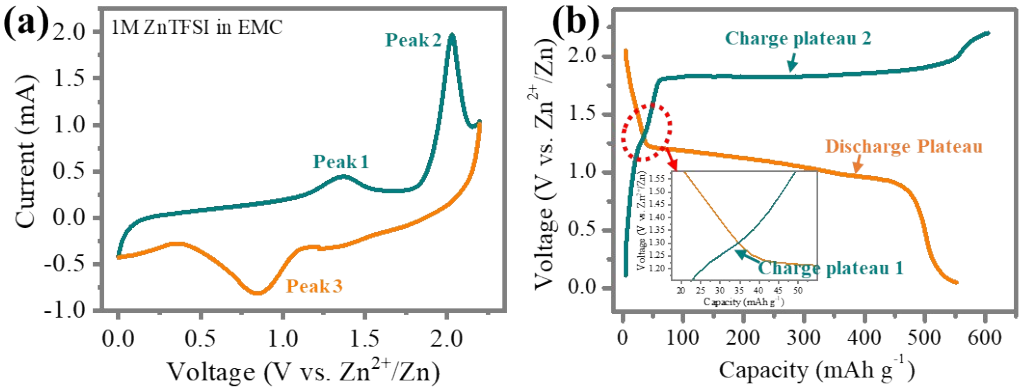

Figure S12. Zn-Se battery based on EMC based electrolyte: a) CV curve and b) GCD curve and the enlarged picture of selected area (inset picture).

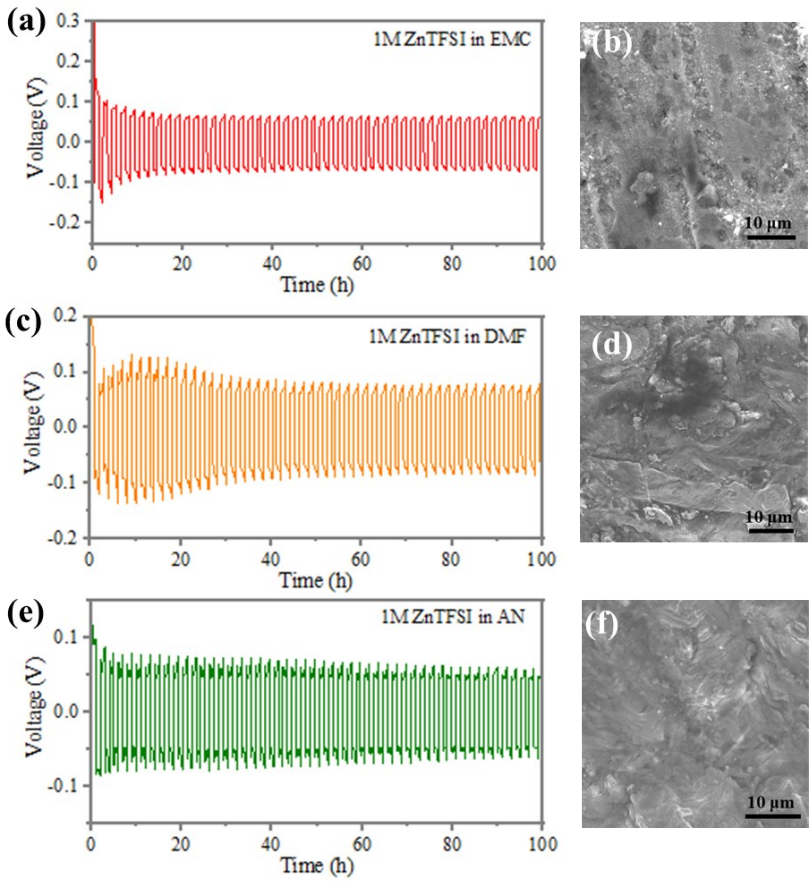

Figure S13. Galvanostatic Zn plating/stripping in Zn/Zn symmetrical cells based on different organic electrolytes (1 mA cm^{-2} and 1mAh cm^{-2}): a) 1M ZnTFSI in EMC and b) the correspondent SEM picture of Zn anode after cycling; c) 1M ZnTFSI in DMF and d) the correspondent SEM picture of Zn anode after cycling; e) 1M ZnTFSI in AN and f) the correspondent SEM picture of Zn anode after cycling.

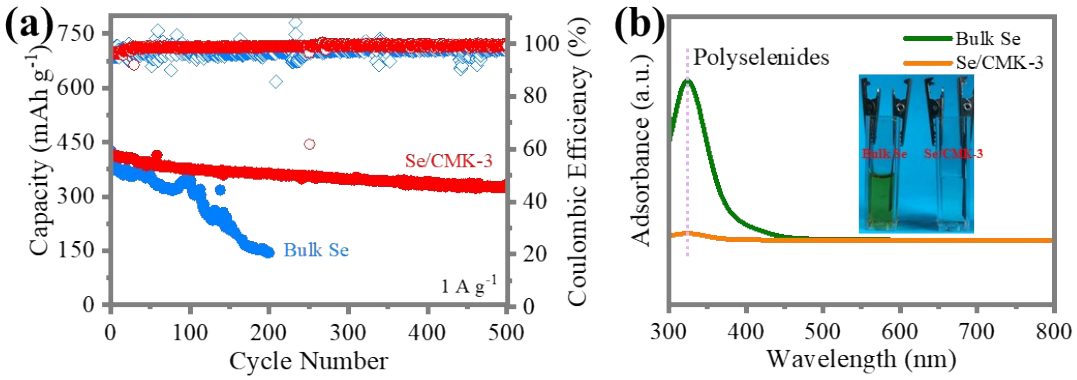

Figure S14. a) Cycling performance of bulk Se powder and Se/CMK-3 based on the organic electrolytes; b) UV-vis test of the electrolytes and the related pictures of cells after 50 cycles (inset).

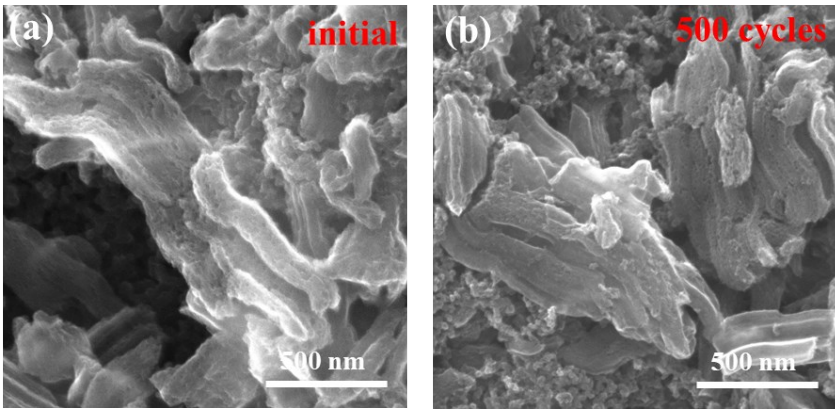

Figure S15. SEM images of Se/CMK-3 at initial state and after 500 cycles under 1 A g^{-1}. No obvious discharging products were produced on the surface of CMK-3 even after 500 cycles.

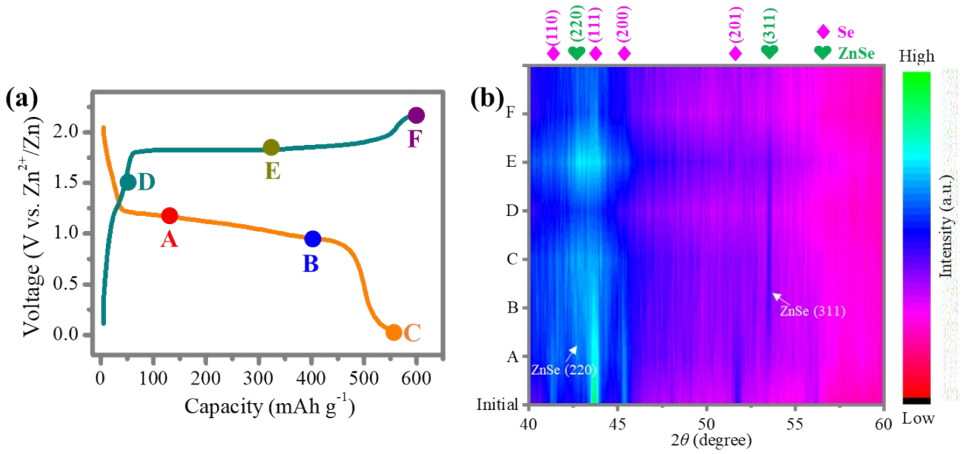

Figure S16. a) GCD profiles of Zn-Se battery based on the EMC electrolyte at 0.1 A g^{-1} and the different color spheres indicate the potentials at which *ex-situ* XRD patterns are collected for structural analysis. b) *Ex-situ* XRD patterns at selected potentials.

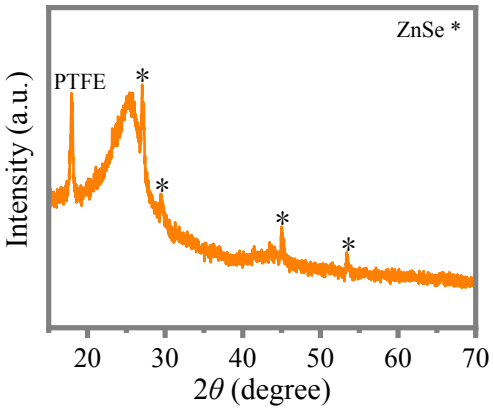

Figure S17. XRD pattern of the Se/CMK-3 cathode after 50 cycles.

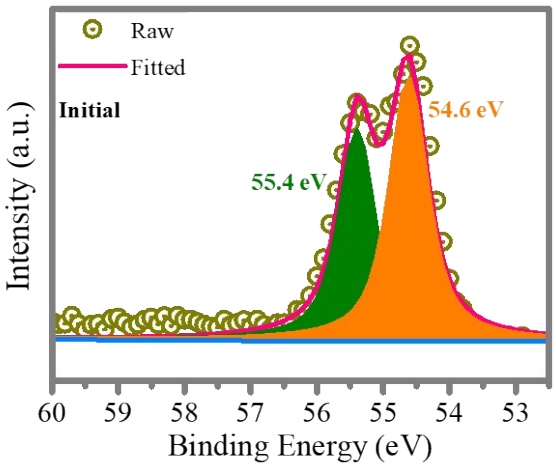

Figure S18. *Ex-situ* core level XPS spectra of Se3d at initial state.

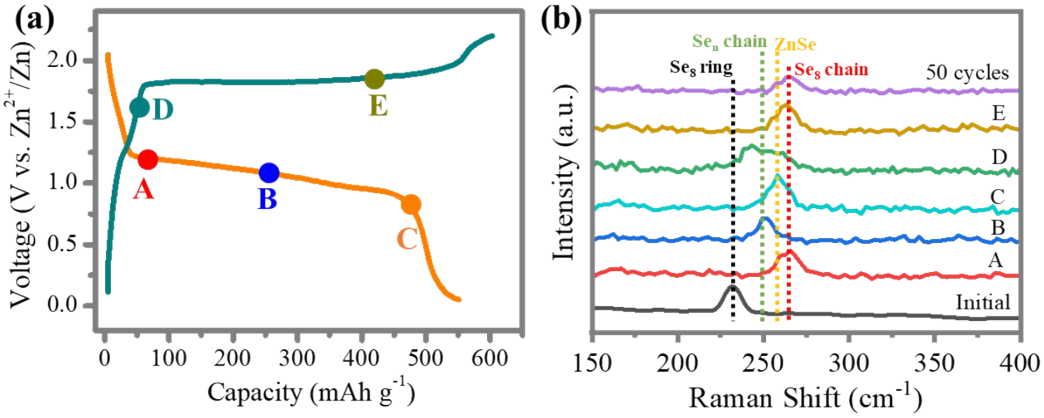

Figure S19. a) GCD profiles of Zn-Se battery based on the EMC electrolyte at 0.1 A g^{-1} and the different color spheres indicate the potentials at which *ex-situ* Raman patterns are collected for structural analysis. b) *ex-situ* Raman patterns at selected potentials.

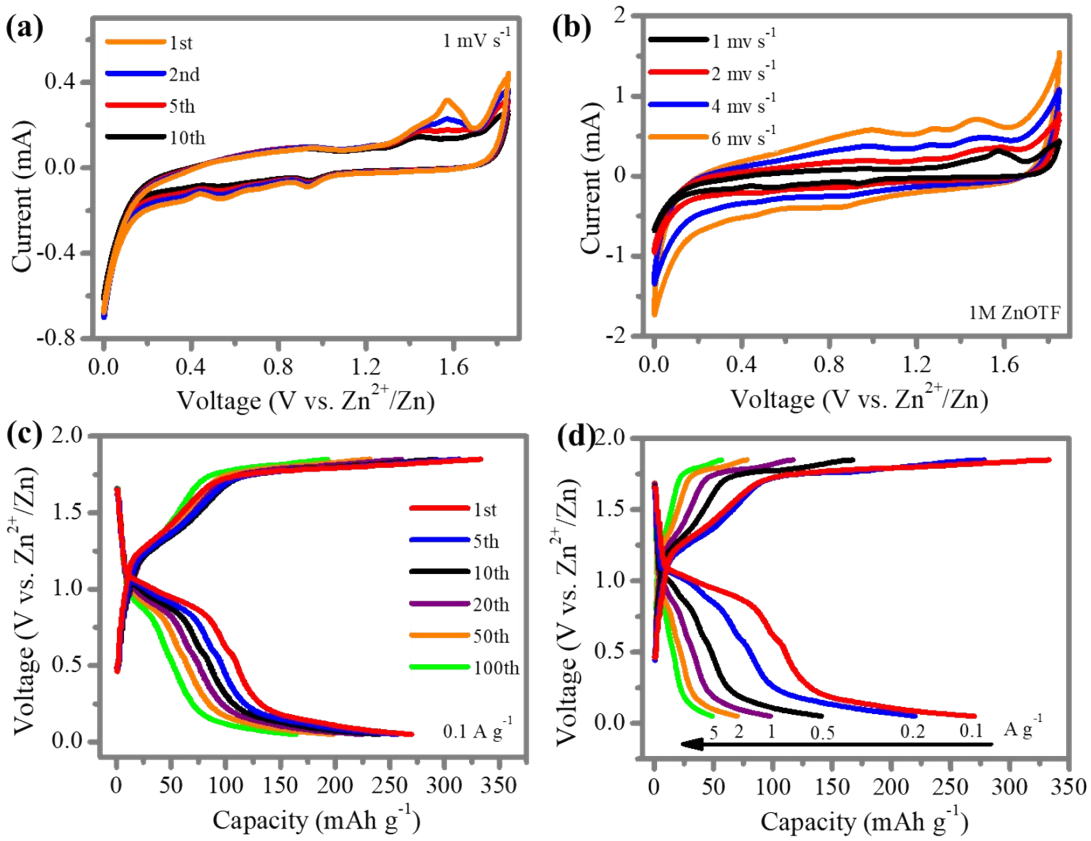

Figure S20. Electrochemical performance of Zn-Se battery based on the electrolytes of 1M ZnTFSI in H_2O: a) CV curves of 1-10 cycles under 1 mV s^{-1}; b) CV curves under different scan rates; c) GCD profiles of 1-100 cycles under 0.1 A g^{-1}; d) GCD profiles under different current density.

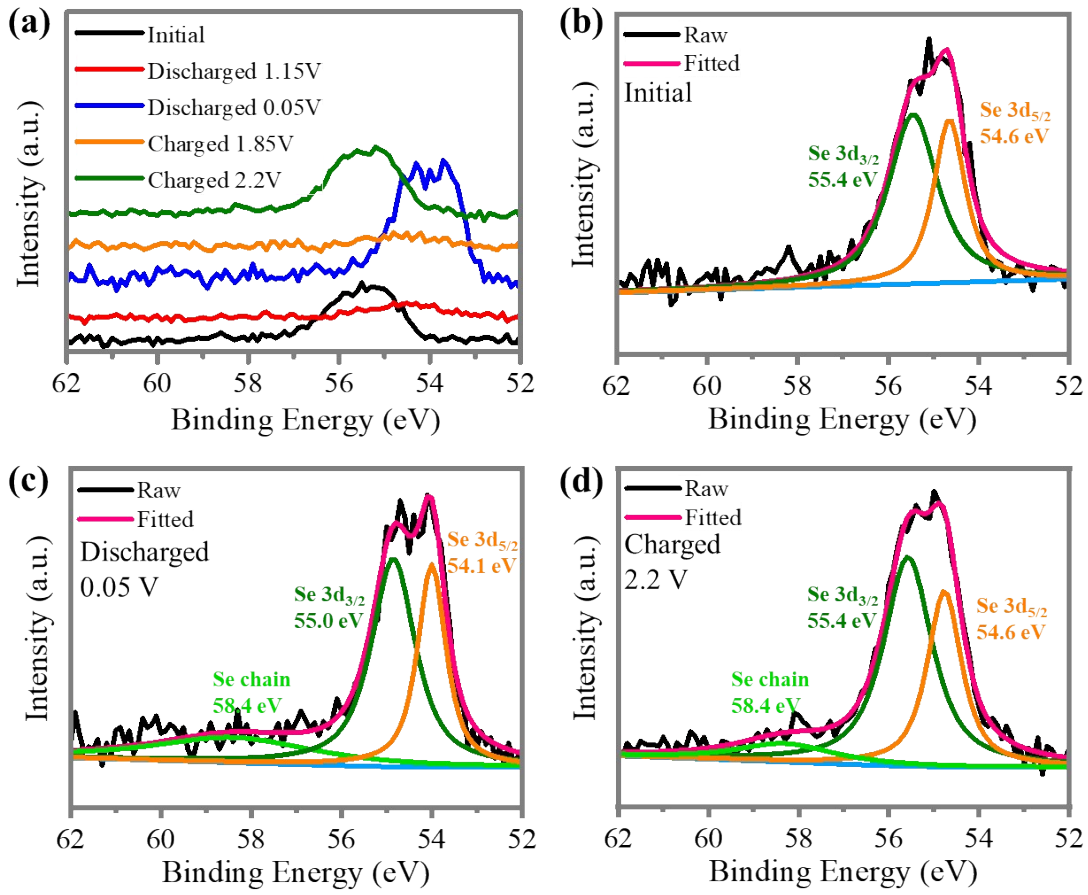

Figure S21. a-d) *Ex-situ* core level XPS spectra of Se3d at selected potentials of Zn-Se batteries based on aqueous electrolytes of 2M ZnTFSI/PEG/water.

Ex-situ XPS was also used to examine the redox process of aqueous Zn-Se batteries at different discharge states (initial, 1.15 V and 0.05 V) and charge states (1.85 V and 2.2 V). Firstly, compared with Se 3d peaks at initial state, a new peak emerges at 58.4 eV at discharged state of 0.05 V. This can be attributed to the presence of chain-like Se_n. In the discharged state of 0.05 V, compared with Se 3d peaks at initial state, obvious Se 3d peak position migrations can be noticed, which results from the conversion from Se^0 to Se^{2-}. Following the charge process, the peak positions of Se 3d shift back, indicating a reversible reaction ($Se_n \leftrightarrow ZnSe$) in the aqueous Zn-Se battery.

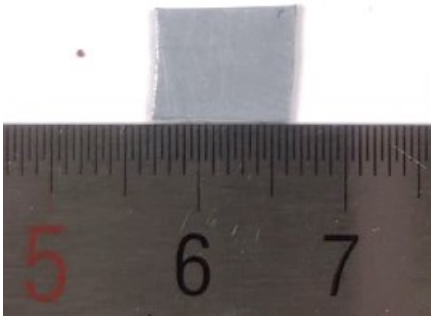

Figure S22. Pictures of Zn anode after 100 cycles in the 2M ZnTFSI/PEG/water electrolyte.

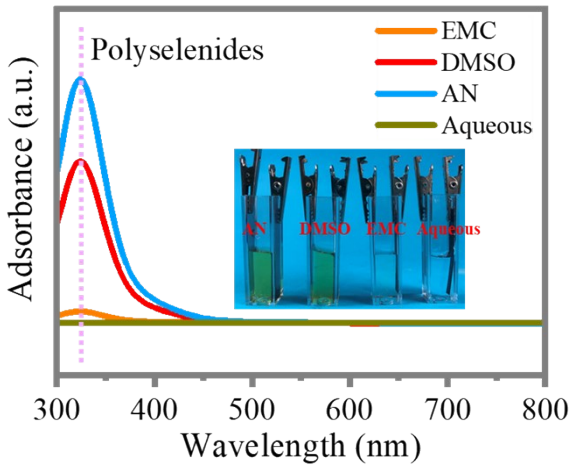

Figure S23. UV-vis spectra of the electrolytes and the related picture of Zn-Se/CMK-3 cells after 50 cycles (inset).

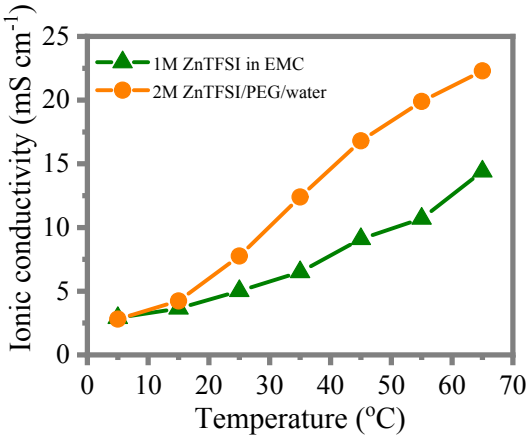

Figure S24. Comparison of ionic conductivity based on different electrolytes.

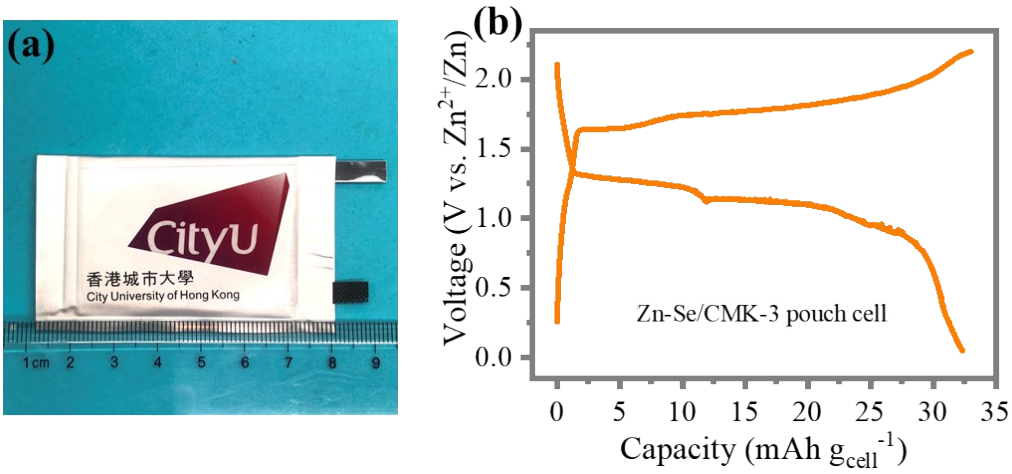

Figure S25. Zn-Se/CMK-3 pouch cell: a) optical picture and b) the related GCD curve (calculated based on the core of the cell).

Table S1. Comparison of specific surface area and pore volume of CMK-3 and Se/CMK-3.

Sample	**specific surface area (m^2 g^{-1})**	**Pore Volume (cm^{-3} g^{-1})**	**Average Pore Size (nm)**
CMK-3	943	1.38	2.13
Se/CMK-3	98	0.07	9.78

References

[1] C. P. Kelly, C. J. Cramer, D. G. Truhlar, The Journal of Physical Chemistry B 2006, 110, 16066.

[2] J. Zhang, M. Dolg, Physical Chemistry Chemical Physics 2016, 18, 3003; J. Zhang, M. Dolg, Physical Chemistry Chemical Physics 2015, 17, 24173.

[3] D. S. Hall, J. Self, J. R. Dahn, The Journal of Physical Chemistry C 2015, 119, 22322.